Proceedings of the ASME 2010 International Design Engineering Technical Conferences & Computers and Information in Engineering Conference
IDETC/CIE 2010
August 15 - 18, 2010, Montreal, Quebec, Canada

DETC2010-28943

AN ENHANCED STABILITY MODEL FOR ELECTROSTATIC COMB-DRIVE ACTUATOR DESIGN

Tristan T. Trutna and Shorya Awtar*
Precision Systems Design Laboratory
Mechanical Engineering, University of Michigan
Ann Arbor MI 48109

ABSTRACT

This paper presents a stability model for predicting the snap-in behavior of electrostatic comb-drive actuators, while taking into account the bearing direction stiffness and error motion of the associated flexure suspension. Error motions typically arise from the flexure suspension kinematics or manufacturing variations. The presented model allows for a more accurate determination of the comb-drive actuator's motion range, limited by snap-in instability, as well as robustness against this instability over the motion range. Ultimately, this model is used as an effective design tool to help evaluate several existing and new flexure suspension geometries for range and robustness.

1. INTRODUCTION AND BACKGROUND

The capacitive or electrostatic comb-drive is a configuration commonly used to sense or induce linear or rotational displacement in MEMS devices. A linear electrostatic comb-drive, illustrated in Fig.1, comprises two sets of electrically isolated conductive comb 'fingers' which have an effective capacitance (C) depending on their number (N), spacing (g), out-of-plane thickness (t), and interdigitation (y_i). While the static comb of fingers is fixed with respect to ground, the moving comb is guided via a suspension so that it can displace primarily in Y direction with respect to the static comb. In MEMS applications of comb-drives, the moving comb suspension is almost always based on flexures [1]. This flexure suspension (also referred to as flexure mechanism or flexure bearing) is designed to provide linearly guided motion and relatively small stiffness (k_y) in the Y direction (or motion direction), along with minimal error motions (e_x) and relatively high stiffness (k_x) in the X direction (or bearing direction). In an ideal scenario, k_y and e_x would approach zero while k_x would approach infinity. However, in practice, this is never the case given the performance tradeoffs between motion range, stiffness, and error motions that exist in flexure mechanisms [2], and manufacturing imperfections that are inherent to micro-fabrication processes [3-4].

Referring to Fig.1, an attractive electrostatic actuation force is induced when a voltage (V) is applied across the static and moving combs. Y displacement of the moving comb is determined by the balance between the Y direction electrostatic (F_{ey}) and suspension spring (F_{sy}) forces.

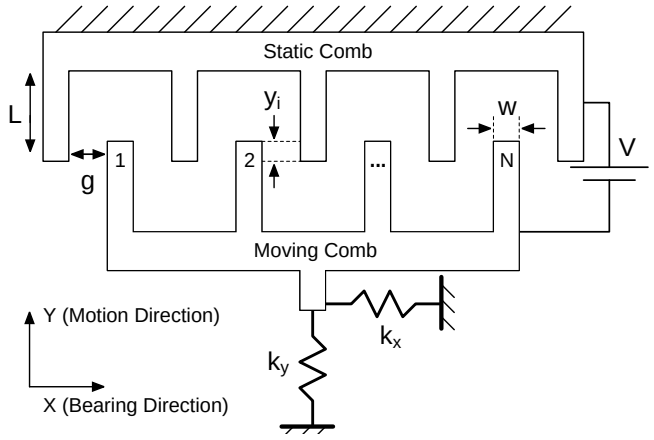

Fig.1 Linear Electrostatic Comb-Drive

Electrostatic comb-drive actuators have been employed in a variety of applications because numerous advantageous attributes. The capacitance of the comb pair varies almost linearly as the moving comb translates along the motion direction. Compared to other MEMS actuators, comb-drives can generally support larger strokes[5]. The small actuator capacitance allows for high speed and low power operation. Furthermore, because comb-drives require no unusual micro-

*Corresponding Author (awtar@umich.edu, 734-615-0285)

fabrication processing, they are easy to incorporate into any monolithic MEMS device. A few representative applications include resonant sensors [6], switches [7], scanning probe microscopy [8], biomolecule and nanoparticle manipulators [9-11], and neural microelectrode positioning [12].

There also exist several challenges in the implementation of electrostatic comb-drives. Large range comb-drive actuators require high operation voltages (often 200V or more) and provide a relatively small actuation force compared to a similarly sized MEMS piezoelectric or thermal actuators [5]. They are also sensitive to dust and other air-borne contaminants, which can be attracted to the charged combs, leading to either a mechanical or electrical failure. However, the most important limitation in the design and use of comb-drive actuators is an instability condition, which arises when the moving comb fingers snap sideways in the bearing direction and contact the static comb fingers at large displacements or driving voltages. This 'snap-in' occurs at a Y displacement where the equilibrium between electrostatic and suspension spring forces becomes unstable. Snap-in can result in a temporary binding of the moving and static comb fingers or permanent damage to the actuator.

Previous work has modeled this instability phenomenon, particularly recognizing the non-linear bearing direction stiffness behavior of flexure suspensions as a primary contributor to snap-in [7, 13]. In addition to bearing direction stiffness reduction, error motions resulting from various sources have been experimentally observed to produce premature snap-in [7]. The primary objective of this paper is to present an analytical closed-model that incorporates the effects of bearing direction stiffness as well as error motions on snap-in instability, so as to accurately predict the motion range and robustness of a comb-drive actuator. Such a stability model can also offer physical insight into the error motion and stiffness characteristics that should be sought in flexure suspension designs to enable large displacement range and robust operation.

The remainder of this paper is organized as follows: In Section 2, we examine prior art in comb-drive actuators and summarize the traditional expressions for stability. In Section 3, we present expressions for actuator stability that take into account manufacturing and kinematic error motions in the bearing direction. In Section 4, a comb-drive flexure suspension design/performance space is presented based on the stability expressions formulated in Section 3. In Section 5, we evaluate existing flexure suspension designs and also propose a set of new designs that potentially offer improvements in motion range, or stability robustness, or both.

2. COMB-DRIVE STABILITY IN THE ABSENCE OF COMB ERROR MOTION

As electrostatic comb-drives were incorporated into devices to produce quasi-static displacements, snap-in instabilities were observed as an unexpected consequence of reducing the gap (g) between moving and static comb fingers in an effort to maximize performance with minimal footprint and driving voltage [14]. While previous work has derived a clear picture of comb-drive stability as a function of driving voltage, displacement, comb gap, and suspension stiffness [7, 13-14], we provide a summary here to serve as the foundation for the subsequent analysis in Section 4.

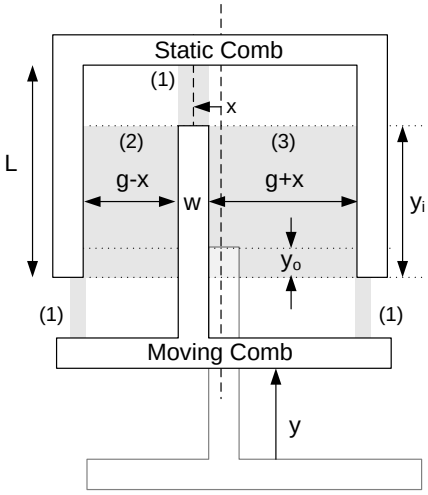

Fig.2 Single Moving Comb Finger

One finger of the moving comb is shown displaced with respect to a pair of Static Comb fingers in Fig.2. The interdigitation (y_i) is simply the sum of the initial (or unactuated) comb finger overlap (y_o) and the motion direction displacement (y). Also shown is a bearing direction perturbation (x) from the nominal comb position.

The capacitance of this comb-drive configuration is approximated by the sum of three parallel plate capacitors, illustrated by the gray areas in Fig. 2.

$$C = \frac{\varepsilon \cdot Area}{gap} = n\left(\underbrace{\frac{2\varepsilon t w}{L - y_i}}_{\text{Comb Tips (1)}} + \underbrace{\frac{\varepsilon t y_i}{g - x} + \frac{\varepsilon t y_i}{g + x}}_{\text{Comb Sides (2,3)}} \right) \tag{1}$$

For typical comb-drive applications, the contribution of the comb tips to the total capacitance is ignored since the length (L) of the comb fingers is much greater than the finger spacing (g), and the finger width (w) is much smaller than their interdigitation (y_i). Having made this assumption, the electrostatic forces are determined by taking the partial derivative of the capacitive potential energy with respect to the motion direction and bearing direction displacements.

$$F_{ey} = \frac{\partial}{\partial y}\tfrac{1}{2}CV^2 = \tfrac{1}{2}n \cdot \varepsilon t\left((g-x)^{-1} + (g+x)^{-1}\right)V^2 \tag{2}$$

$$F_{ex} = \frac{\partial}{\partial x}\tfrac{1}{2}CV^2 = \tfrac{1}{2}n \cdot \varepsilon t y_i\left((g-x)^{-2} - (g+x)^{-2}\right)V^2 \tag{3}$$

The quasi-static operation of a comb-drive actuator is determined by the equilibrium between these electrostatic forces and the suspension spring forces given by $k_y y$ and $k_x x$, in the motion and bearing directions, respectively. It may be easily shown from Eq.(2) that there is a single equilibrium position in the Y direction for a given voltage V, and that this equilibrium

is always stable. The equilibrium position(s) in the X direction are shown graphically in Fig.3, which plots the bearing direction spring and electrostatic forces for x values from $-g$ to g for two different spring suspensions ("Spring 1" and "Spring 2") for a given actuation voltage V.

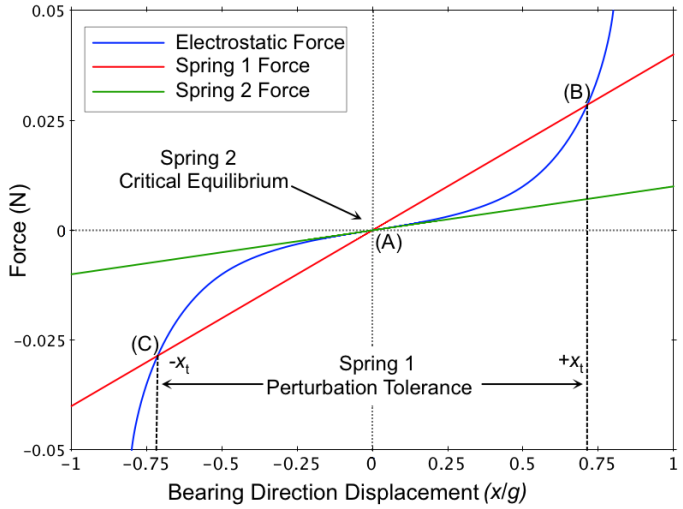

Fig.3 Bearing Direction Comb Drive Equilibrium Positions

Clearly, when the suspension stiffness in the bearing direction (k_x) is greater than a certain critical value, such as in the case of Spring 1, there are three equilibrium positions in the X direction: $x = 0$ (A) and $x = \pm x_t$ (B and C). The stability of these equilibrium positions can be determined by perturbing the moving comb slightly and examining the resulting electrostatic and spring forces. The equilibrium at $x = 0$ is stable because the restoring spring force is greater than the non-restoring electrostatic force. Mathematically, this may be stated as the slope of the spring force with respect to x (or stiffness k_x) being greater than the slope of the electrostatic force at the point of interest. The other equilibrium points at $x = \pm x_t$ are therefore unstable since the electrostatic force slope greatly exceeds the spring stiffness at these positions. As the spring stiffness is decreased, the two unstable equilibria, (B) and (C), move towards the origin (A), until a critical spring stiffness is reached at which there is a single marginally stable equilibrium at $x = 0$. Spring 2 corresponds to this critical spring stiffness k_{xc}, which is simply given by the slope of the electrostatic force at $x = 0$. This critical stiffness can be calculated analytically from Eq. (3) as follows:

$$k_{xc} = \left(\frac{\partial F_{ex}}{\partial x}\right)_{x=0} = \frac{2n\varepsilon t\left(y+y_o\right)}{g^3}V^2 \qquad (4)$$

This implies that a comb-drive actuator should be stable at any y displacement as long as the bearing direction stiffness exceeds the critical spring stiffness given above. This conclusion is consistent with a number of previous publications [7, 13-14]. Solving Eq.(4) simultaneously with the Y direction force equilibrium:

$$k_y \cdot y = n \cdot \varepsilon t\left((g-x_c)^{-1}+(g+x_c)^{-1}\right)V^2 \qquad (5)$$

yields a stability condition in terms of only the suspension stiffness in the motion and bearing directions, motion direction displacement and initial interdigitation, and finger gap.

$$\frac{k_x}{k_y} \geq \frac{k_{xc}}{k_y} = \frac{y\left(y+y_o\right)}{g^2} \qquad (6)$$

It is interesting to note that while this expression is based on the comb-drive architecture of Fig.1, it is largely independent of specific geometric or physical parameters associated with the electrostatic comb-drive, other than g and y_o. Actuation voltage, comb finger dimensions, material choice, etc. do not appear in this expression.

In practice k_x should be greater than k_{xc} to provide a certain margin of robustness against instability. Referring back to Fig.3, when $k_x > k_{xc}$, there is a single stable equilibrium position at $x = 0$, with a $\pm x_t$ margin of stability. In other words, the moving comb will return to its stable equilibrium position for any X direction perturbation less than $\pm x_t$. If the perturbation exceeds $\pm x_t$, the moving comb will snap in to the static comb, in spite of k_x being greater than k_{xc}. Here, we define perturbation as an unexpected displacement that might arise due to an external disturbance force, for example. x_t can be derived in terms of gap g, actual bearing direction stiffness k_x, and the critical bearing direction stiffness k_{xc}:

$$\frac{x_t}{g} = \pm\sqrt{1-\sqrt{\frac{k_{xc}}{k_x}}} \qquad (7)$$

This expression shows that by maintaining a 10% excess bearing direction stiffness, the comb-drive is tolerant to perturbations that are ±22% of g. Once again, the above result is independent of the comb drive physical and geometric parameters. It should be noted that the results of this section assume a situation when there are no error motions in the X direction due to either the flexure suspension kinematics or manufacturing imperfections.

3. COMB-DRIVE STABILITY IN THE PRESENCE OF COMB ERROR MOTION

While the stability analysis in Section 2 has been discussed in depth in the literature [7, 13-15], the contribution of comb error motion (e_x) to comb-drive instability has not been explicitly presented in closed form. This error motion is defined as any undesired but repeatable bearing direction displacement or misalignment between the moving and static comb from the nominal symmetric position ($x = 0$) induced by sources independent of the electrostatic operation of the actuator. Examples include an initial misalignment resulting from the manufacturing process, an error motion resulting from the flexure suspension kinematics [2], or an error motion resulting from manufacturing variations (such as inconsistent flexure beam profiles).

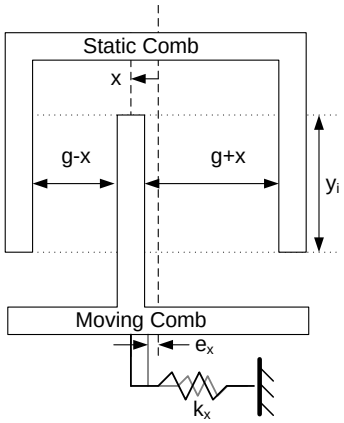

Fig. 4 Comb Finger with Error Motion (e_x)

For any given motion direction displacement y, the bearing direction motions are shown in Fig.4. e_x is the total error motion. x is the absolute displacement of the moving comb with respect to the theoretical nominal position and includes this error motion, contribution from the electrostatic forces, and any unexpected perturbations. Therefore, the nominal position for the bearing direction spring is e_x and resulting spring force is offset adjusted accordingly [16]. The electrostatic force is still dependent on the absolute position x, and is unaffected by e_x. The resulting bearing direction force balance may therefore be written as:

$$k_x(x-e_x)=\tfrac{1}{2}n\cdot\varepsilon t y_i\left((g-x)^{-2}-(g+x)^{-2}\right)V^2 \tag{8}$$

This force balance is illustrated graphically in Fig.5. The blue line represents the electrostatic force, which is the right-hand side in the above equation. The red line represents the spring force, with stiffness $k_x > k_{xc}$ (Eq.(6)), in the presence of error motion (e_x).

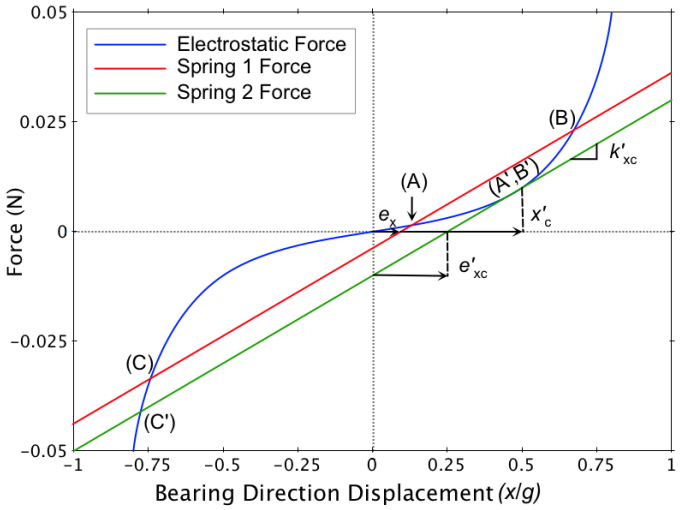

Fig. 5 Bearing Direction Comb Drive Equilibrium Positions in the presence of Error Motions

For a relatively small e_x, one can see that there are still three equilibrium positions: the central position (A), which is no longer at $x = 0$, is stable; the outer two positions (B) and (C) are unstable. The margin of stability of equilibrium (A) is given by $\{-x_{tC}, x_{tB}\}$. In other words, any quasi-static perturbation of the moving comb within this range will cause it to go back to equilibrium (A), and any perturbation beyond this range with cause the moving to snap into the static comb.

For a larger e_x, the equilibrium positions (A) and (B) will be closer together, and the associated perturbation range of stability will be smaller. For a certain large enough positive direction error motion (e_x), represented by the green line in Fig.5, these two equilibrium positions will coincide (A' and B'). In that case, all three equilibrium positions will be unstable and snap-in will happen upon the slightest of perturbation. Thus, the margin of stability in terms of allowed perturbation becomes zero.

Fig.5 makes it graphically evident that comb-drive snap-in instability is not only determined by the bearing direction spring stiffness but also the error motion. The limit of stable operation is mathematically given by the condition when the slopes of the electrostatic force and spring force are equal:

$$k_x=n\cdot\varepsilon t y_i\left((g-x)^{-3}+(g+x)^{-3}\right)V^2 \tag{9}$$

Equations (8) and (9) may be solved simultaneously to determine the critical operating condition of marginal stability at which the bearing direction stiffness is $k_{xc}^{(e)}$ and the unstable equilibrium position in x_c, for a given error motion e_x:

$$e_x=\frac{4x_c^3}{g^2+3x_c^2} \tag{10}$$

$$\Rightarrow x_c=\frac{e_x^2}{4\sqrt[3]{8g^2e_x+4\sqrt{4g^4e_x^2+g^2e_x^4}+e_x^3}}+\frac{1}{4}\sqrt[3]{8g^2e_x+4\sqrt{4g^4e_x^2+g^2e_x^4}+e_x^3}+\frac{e_x}{4} \tag{11}$$

$$k_{xc}^{(e)}=n\cdot\varepsilon t y_i\left((g-x_c)^{-3}+(g+x_c)^{-3}\right)V^2 \tag{12}$$

Eq.(12) may be solved simultaneously with the Y direction force equilibrium relation Eq.(5) to yield the following condition for stable operation:

$$\frac{k_x}{k_y}\geq\frac{k_{xc}^{(e)}}{k_y}=\frac{y\cdot(y+y_o)}{g^2}\left[\frac{1+\frac{3x_c^2}{g^2}}{\left(1-\frac{x_c^2}{g^2}\right)^2}\right] \tag{13}$$

Eqs. (11) and (13), considered together, present a closed form condition for comb-drive stability in the presence of bearing direction error motions. These analytical results are consistent with previously reported experimental observations [7]. A few important observations can be made here:

1. Eq.(11) provides the single real solution of the cubic Eq.(10). These two relations show that the bearing direction equilibrium position at snap-in x_c is uniquely defined as a function of comb finger gap g and error motion e_x, and vice-versa. Even though non-linear and unwieldy, these relations are entirely independent of the bearing or motion direction stiffness, motion

direction displacement, driving voltage, and any other comb-drive geometric or physical parameters.

2. The stability condition in this case, Eq.(13), is analogous to Eq.(6) in Section 2. In fact, for $e_x = 0$, the critical equilibrium position x_c becomes 0 as per Eq.(11), and $k_{xc}^{(e)}$ reduces to k_{xc}. However, for non-zero e_x, $k_{xc}^{(e)}$ is always greater than k_{xc}. This implies that in the presence of bearing direction error motion, the requirement placed on the bearing direction stiffness to avoid snap-in instability is higher. While the prior work [7] recognizes the non-zero critical equilibrium position, x_c, and its influence on the critical stiffness as per Eq.(13), it does not present an explicit closed-form dependence of the critical equilibrium position x_c on the error motion e_x, given by Eq.(11). Elsewhere, an empirical and slightly inaccurate relation between x_c and e_x has been proposed [16].

4. COMB-DRIVE FLEXURE SUSPENSION DESIGN SPACE FOR OPTIMAL RANGE AND ROBUSTNESS

Eq.(13) reveals that for the comb-drive architecture in Fig.1, the stability condition that limits the actuator's motion range depends primarily on the flexure suspension design. The only relevant attribute of the electrostatic comb-drive that features in this condition is the comb finger gap g. While a small gap is generally desirable to produce greater actuation forces in a smaller foot-print for a given driving voltage, its lowest practical limit is generally dictated by the micro-fabrication process. Once this value has been identified, the maximum achievable motion range before snap-in depends simply on the ratio of the bearing direction stiffness and motion direction stiffness, and the bearing direction error motion, as per Eq.(13). This closed-form condition may therefore be used for determining the flexure suspension design specifications for a desired actuator motion range, or alternatively, the motion range and stability robustness that can be achieved by employing a certain flexure suspension design.

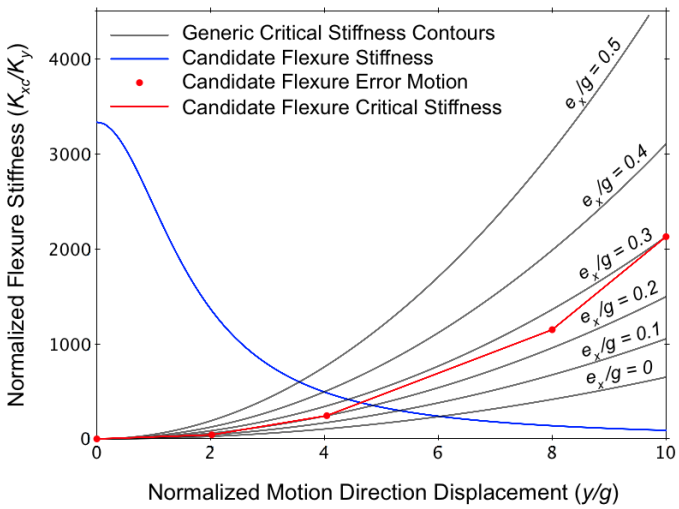

Fig. 6 Comb Drive Flexure Suspension Design Space

In general, the motion direction stiffness of a flexure suspension remains relatively constant with respect to the motion direction displacement y, whereas its bearing direction stiffness and error motions vary with y [2]. For stable operation, Eq.(13) should remain valid at each motion direction displacement y; the smallest y for which this condition fails represents the snap-in position and the actuator's displacement limit. This stability condition may be graphically represented via a contour map of critical bearing stiffness $k_{xc}^{(e)}$ as a function of y / g for various constant values of e_x / g (Fig.6). For a chosen nominal value of g (1 μm, in this case), this contour map remains invariant regardless of the comb-drive specifics and flexure suspension design. This contour plot may then be used to evaluate a candidate flexure suspension design, as long as its bearing direction stiffness and error motion are known (analytically, numerically, or experimentally).

As an example, Fig.6 presents the stability performance of a candidate suspension design (a symmetric double parallelogram flexure, discussed later). The blue line represents its k_x / k_y ratio versus displacement y. Assuming that the bearing direction error motion is known at five discrete y displacement values, the corresponding critically required bearing stiffness values are picked from the e_x / g contours. These points may be connected (red line) to provide a plot of $k_{xc}^{(e)}$ / k_y versus y. The theoretical maximum displacement range of a comb-drive actuator that employs this candidate flexure suspension is simply given by the intersection of the blue and red lines.

The ratio between the critical stiffness required to prevent snap-in and the bearing stiffness provided by the suspension, ($k_{xc}^{(e)}$/k_x), may be used as a metric for instability (I). For small y displacements, I is less than 1, and at the point of intersection of the red and blue lines, the margin of stability becomes zero and I becomes 1 (or 100%).

5. PROPOSED FLEXURE SUSPENSION DESIGNS

Given the various benefits of electrostatic comb-drive actuators, reducing or delaying the onset of snap-in instability has been an ongoing goal in MEMS research. A wide variety of approaches have been employed, which include feedback control [17], various comb finger geometries [7, 18], actuator cascading [19-20], and clever flexure suspension designs [7, 16, 21].

Fig.6 shows that by simply increasing g, the instability occurs at a larger y displacement, thus increasing the actuator range. However, as per Eq.(5), increasing g also implies that to achieve the necessary actuation force, either a larger drive voltage is needed or a larger number of comb teeth are required, which leads to larger device footprint. Thus, there is a clear trade-off associated with simply varying the gap g to improve range. It is important to note that this comb finger gap variation is entirely independent of the flexure suspension design.

Furthermore, Fig.6 shows that any finite bearing direction error motion e_x increases the required or critical bearing direction stiffness to prevent snap-in. Also, it is clear that a high

bearing stiffness is required at larger y displacements. In fact, the critical bearing direction stiffness increases quadratically with y, as per Eqs. (6) and (13). This is the opposite of what most traditional flexure suspension designs offer. For example, Fig.6 shows the bearing stiffness provided by a symmetric double parallelogram flexure (DPF) suspension (illustrated in Fig.7a), which is maximum at $y = 0$ and drops significantly with increasing y [2]. Consequently, a DPF suspension will succumb to snap-in instability for relatively small displacements. A good flexure suspension design would be one that offers low inherent error motions and high bearing stiffness at larger displacements; the bearing stiffness at very low displacements need not necessarily be very high.

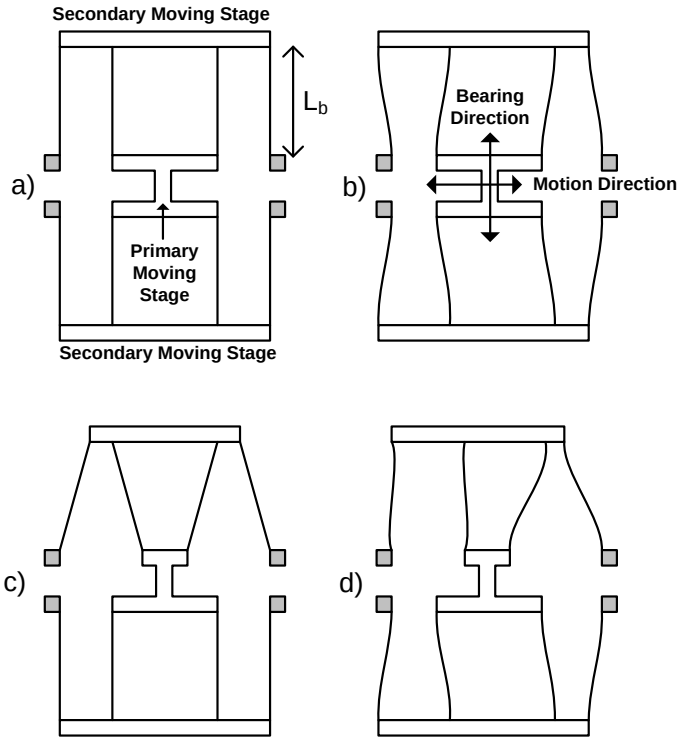

Fig. 7 a) Double Parallelogram Flexure (DPF), b) Symmetric Pre-bent DPF, c) Asymmetric Tilted-Beam Flexure (TBF), and d) Asymmetric Pre-bent TBF

An important development in the comb-drive flexure suspension design has been the use of pre-bent beams in the DPF geometry [7, 16, 21], as shown in Fig.7b. The pre-bending of beams ensures that the maximum bearing direction stiffness does not occur at $y = 0$, but instead at a y displacement where the pre-bent beams are deformed into a "straight" shape. Fig.8 illustrates the bearing direction stiffness variation of the DPF (red line) and pre-bent DPF (blue line). All physical dimensions used in this figure are from a previous publication [7]. The y location of the stiffness peak directly depends on the degree of pre-bending incorporated in the beams. Also shown in this figure is the critical bearing stiffness without and with error motions (dashed black lines). While both designs exhibit theoretically zero inherent kinematic error motions because of their symmetric geometry, typical manufacturing errors [7] are included in this figure.

Since the pre-bent DPF provides greater stiffness at large y displacements, it is clear from Fig.8 that it delays the onset of snap-in instability and provides greater range, with and without error motions. This has been experimentally corroborated in the past [7, 16, 21]. In this particular example, the pre-bent DPF can theoretically achieve a range close to $0.15L_b$, whereas the DPF can only achieve $0.07L_b$. However, given narrow shape of the bearing stiffness curve, the margin of stability in case of the pre-bent DPF becomes small over significant segments of the actuator stroke (see $y/L_b = 0.07$ to 0.10 in Fig. 8). This low margin of stability leads to a lack of robustness: unexpected errors in manufacturing could shift the peak stiffness location, unpredicted error motions could increase the required critical stiffness, environmental disturbances could perturb the moving comb, etc. Any of these scenarios would lead to snap-in at displacements much lower than the predicted maximum range.

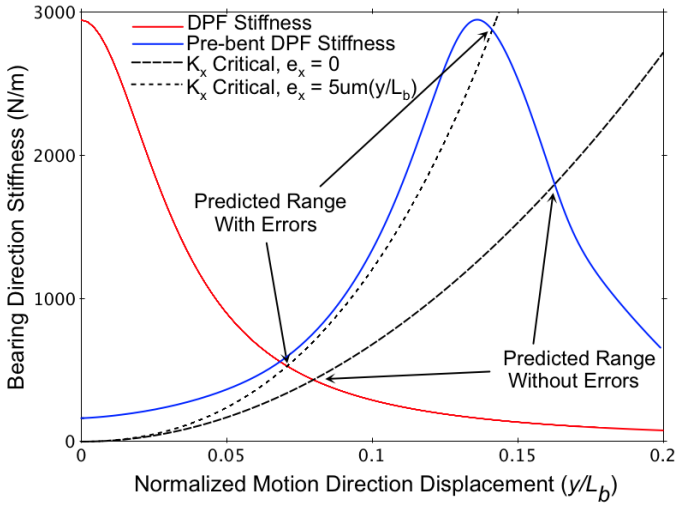

Fig.8 DPF and Pre-bent DPF Actuator Range Comparison

In both the DPF as well as pre-bent DPF suspension designs, the rapid degradation in bearing direction stiffness from its maximum value with increasing motion direction displacement is the major limitation. In the former case, the actuator stroke is limited while in the latter case robustness over an otherwise larger stroke is adversely affected. It is therefore desirable to explore flexure suspension designs, in which the bearing direction stiffness does not drop with motion direction displacement, and if it does the stiffness degradation is not as steep. Additionally, any new designs should ideally maintain a device foot-print similar to the existing designs.

The first step in the process of seeking new suspension designs is to understand the physical reasoning behind the above seen bearing direction stiffness behavior of the DPF. The DPF suspension design of Fig.7a is made up of two identical double parallelogram flexure modules (above and below a horizontal line of symmetry). Each module by itself represents an under-constrained design comprising of a primary moving stage (which is attached to the moving comb) and a secondary

moving stage. Even when the primary stage is held fixed at a non-zero *y* displacement, the secondary stage is free to move in the Y direction. In fact the application of a bearing direction force causes this Y motion of the secondary stage even as the primary stage is held fixed. This is due to the non-linear load-stiffening or softening of the parallelogram flexures within each double parallelogram flexure module. This Y direction displacement of the secondary stage leads to a discrepancy between the kinematic contraction of the beams along their length in the inner and outer parallelogram flexures within each double parallelogram flexure module. This discrepancy produces an additional displacement of the primary motion stage in the bearing direction. Since this displacement occurs in response to a bearing direction force, it represents an increased compliance or reduced stiffness. Because the kinematic contraction increases quadratically with Y displacement of the primary and secondary stages, the bearing direction compliance also increases quadratically with *y*. A more detailed quantitative and qualitative description of this phenomenon is provided in the prior art [2]. The same reasoning also explains the drop in bearing direction stiffness in the pre-bent DPF, except that the maximum stiffness location with respect to *y* is off-set by the amount of pre-bending incorporated in the beams (Fig.8).

To prevent or limit this bearing direction stiffness drop, it is therefore critical to arrest the free Y direction motion of the secondary stages in response to a bearing direction force on the primary stage. This may be accomplished via an asymmetric tilted-beam flexure (TBF) suspension design shown in Fig.7c, first proposed in [2]. The bottom half of this suspension design is the traditional double parallelogram flexure module, and the top half is a double tilted-beam flexure module. The two halves of the suspension serve distinct and mutually complementary roles. The tilted beams of the double tilted-beam flexure module make it an exactly constrained design. In other words, if one were to specify the *y* displacement and rotation of the primary stage, the secondary stage in this module would be completely constrained with little freedom to move in Y direction or rotate even in the presence of a bearing direction load on the primary stage. A more detailed physical and analytical discussion of this behavior is provided in [2]. Thus, the steep drop of the bearing direction stiffness of this module can be restricted, if only the rotation of the primary motion stage could be constrained. This requirement is met by the double parallelogram flexure module on the lower half of this suspension design. Even though this latter module does not help with the bearing direction stiffness, for reasons described above, it provides a high rotational stiffness to constrain the rotation of the primary stage. Thus, the two units acting in conjunction help achieve better bearing direction stiffness. The resulting stiffness variation with *y* is illustrated graphically in Fig.9. However, it is important to note that the asymmetry in this design induces greater inherent or kinematic error motions in the bearing direction. Therefore, as per Eq.(13), the critical or required stiffness is also greater.

As expected, the asymmetric TBF produces a wider stiffness profile with a more gradual decay in the bearing stiffness (solid red line) with increasing *y* displacements. The required critical stiffness based on the previously assumed manufacturing errors and the kinematic errors inherent in this design is also shown (dashed red line). For comparison, the bearing stiffness (solid blue line) and the critical stiffness based on manufacturing errors only (dashed blue line) associated with the pre-bent DPF are also shown in this figure.

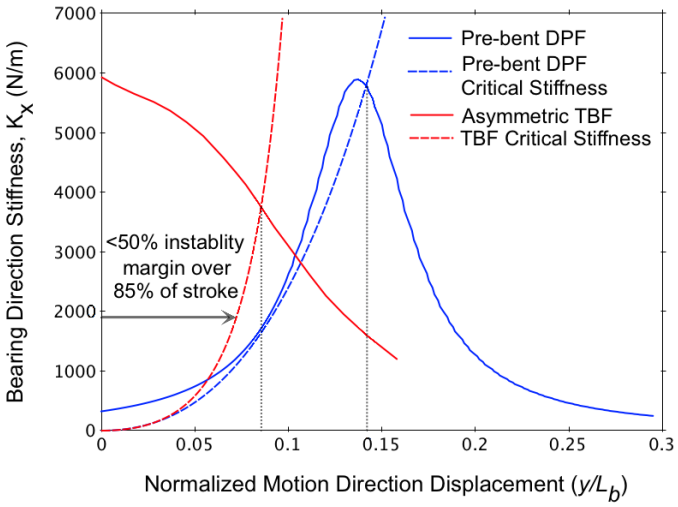

Fig. 9 Pre-bent DPF and asymmetric DPF Actuator Range and Robustness Comparison

It is evident in Fig.9 that because the asymmetric TBF produces more error motions, the critical stiffness associated with this design grows at a greater rate than in the case of the pre-bent DPF. However, its better bearing direction stiffness characteristics produce a higher margin of stability over the stroke of the actuator. Examining the performance of these flexures in terms of their instability (*I*), defined in Section 4 as the ratio of their critical and flexure stiffness, over their full strokes provides a clearer picture of actuator performance and robustness.

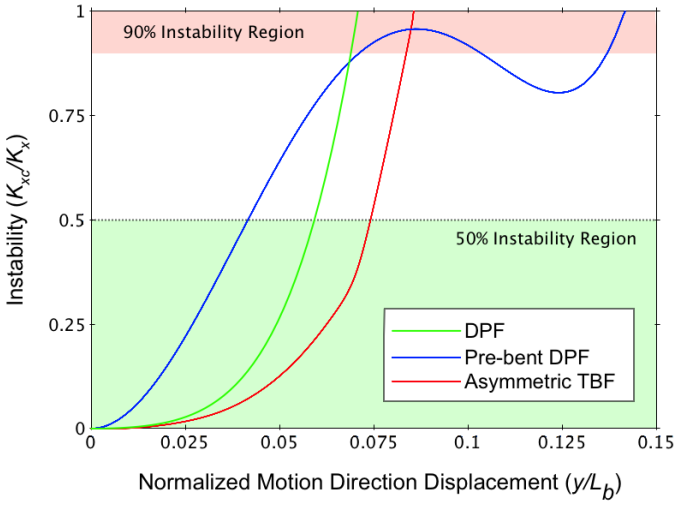

Fig. 10 DPF, Pre-bent DPF and asymmetric TBF Instability Comparison

Fig.10 presents such a comparison between the three flexure suspension designs discussed so far – DPF, pre-bent DPF, and asymmetric TBF. Even though it offers the largest range, the pre-bent DPF has a region of high instability between y/L_b = 0.07 to 0.1. On the other hand, the asymmetric TBF does not produce as large a motion range; however, its range is still 20% greater than that provided by the traditional DPF. More importantly, the asymmetric TBF maintains an instability (I) of less than 50% over most of its motion range. Thus, in applications where comb-drive robustness is of primary concern, an asymmetric TBF can offer an ideal compromise between enhanced range and robustness. Upon further optimization of the asymmetric TBF geometry, we expect further improvements in range with a similar instability profile.

Drawing on the increased range associated with the pre-bent DPF and the enhanced robustness of the asymmetric TBF, the next iteration in the suspension design for comb-drive actuators is shown in Fig.7d. This novel design incorporates the pre-bent beams of Fig.7b and the asymmetric geometry of Fig.7c. Preliminary analysis of this asymmetric pre-bent TBF suspension design indicates a simultaneous shifting of the stiffness profile to increase range, and widening of the stiffness profile to improve robustness.

6. CONCLUSIONS AND FUTURE WORK

Enhancing the range and robustness of comb-drive actuators presents a significant design challenge and requires a complete understanding of comb-drive limitations. While the effect of bearing direction error motions on the snap-in instability, and therefore actuator range, has been previously studied, in this paper we have presented explicit closed-form stability conditions that take into account both the bearing direction stiffness and error motion. Based on this model, a graphical comb-drive flexure suspension design space is presented, and employed in evaluating existing and new flexure suspension designs. The asymmetric pre-bent TBF design proposed here holds the potential for superior range and robustness. Our on-going plans include detailed analytical predication of this improved performance and experimental validation of micro-fabricated devices.

REFERENCES

[1] Jaecklin, V., Linder, C., De Rooij, N., Moret, J., Bischof, R., and Rudolf, F., 1992, "Novel polysilicon comb actuators for XY-stages," IEEE Micro Electro Mechanical Systems, 1992, MEMS'92, Proceedings. An Investigation of Micro Structures, Sensors, Actuators, Machines and Robot, pp. 147-149.

[2] Awtar, S., Slocum, A. H., and Sevincer, E., 2007, "Characteristics of beam-based flexure modules," Journal of Mechanical Design, 129(6), pp. 625-639.

[3] Chen, B. T., and Miao, J. M., 2007, "Influence of deep RIE tolerances on comb-drive actuator performance," Journal of Physics D-Applied Physics, 40(4), pp. 970-976.

[4] Chen, K., Ayun, A., Zhang, X., and Spearing, S., 2002, "Effect of process parameters on the surface morphology and mechanical performance of silicon structures after deep reactive ion etching (DRIE)," Journal of Microelectromechanical Systems, 11(3), pp. 264-275.

[5] Bell, D. J., Lu, T. J., Fleck, N. A., and Spearing, S. M., 2005, "MEMS actuators and sensors: observations on their performance and selection for purpose," Journal of Micromechanics and Microengineering, 15(1), pp. 153-S164.

[6] Tang, W. C., Nguyen, T. C. H., Judy, M. W., and Howe, R. T., 1990, "Electrostatic-comb drive of lateral polysilicon resonators," Sensors and Actuators A: Physical, 21(1-3), pp. 328-331.

[7] Grade, J., Jerman, H., Kenny, T., Inc, I., and San Jose, C., 2003, "Design of large deflection electrostatic actuators," Microelectromechanical Systems, Journal of, 12(3), pp. 335-343.

[8] Indermühle, P., Jaecklin, V., Brugger, J., Linder, C., De Rooij, N., and Binggeli, M., 1995, "AFM imaging with an XY-micropositioner with integrated tip," Sensors & Actuators: A. Physical, 47(1-3), pp. 562-565.

[9] Mukundan, V., and Pruitt, B. L., 2009, "MEMS Electrostatic Actuation in Conducting Biological Media," Journal of Microelectromechanical Systems, 18(2), pp. 8.

[10] Harouche, I. P. F., Shafai, C., and Gordon, R., 2006, "Design and simulation of a microtweezers using a controlled displacement comb drive," 2006 Canadian Conference on Electrical and Computer Engineering, Vols 1-5, pp. 136-138.

[11] Liu, X. Y., Tong, J. H., and Sun, Y., 2007, "Millimeter-Sized Nanomanipulator with Sub-Nanometer Positioning Resolution and Large Force Output," 2007 7th IEEE Conference on Nanotechnology, Vol 1-3, pp. 456-459.

[12] Muthuswamy, J., Okandan, M., Jain, T., and Gilletti, A., 2005, "Electrostatic microactuators for precise positioning of neural microelectrodes," Ieee Transactions on Biomedical Engineering, 52(10), pp. 1748-1755.

[13] Legtenberg, R., Groeneveld, A., and Elwenspoek, M., 1996, "Comb-drive actuators for large displacements," Journal of Micromechanics and microengineering, 6(3), pp. 320-329.

[14] Hirano, T., Furuhata, T., Gabriel, K. J., and Fujita, H., 1992, "Design, fabrication, and operation of submicron gap comb-drive microactuators," Journal of Microelectromechanical Systems, 1(1), pp. 52-59.

[15] Huang, W., and Lu, G., 2004, "Analysis of lateral instability of in-plane comb drive MEMS actuators based on a two-dimensional model," Sensors & Actuators: A. Physical, 113(1), pp. 78-85.

[16] Chen, C., and Lee, C., 2004, "Design and modeling for comb drive actuator with enlarged static displacement," Sensors and Actuators A: Physical, 115(2-3), pp. 530-539.

[17] Borovic, B., Lewis, F. L., Liu, A. Q., Kolesar, E. S., and Popa, D., 2006, "The lateral instability problem in electrostatic comb drive actuators: modeling and feedback control," Journal of Micromechanics and Microengineering, 7(1), pp. 1233.

[18] Jensen, B. D., Mutlu, S., Miller, S., Kurabayashi, K., and Allen, J. J., 2003, "Shaped comb fingers for tailored electromechanical restoring force," Journal of Microelectromechanical Systems, 12(3), pp. 373-383.

[19] Chiou, J. C., Lin, Y. J., and Kuo, C. F., 2008, "Extending the traveling range with a cascade electrostatic comb-drive actuator," Journal of Micromechanics and Microengineering, 18(1), pp.
[20] Hou, M. T.-K., Huang, G. K.-W., Huang, J.-Y., Liao, K.-M., Chen, R., and Yeh, J.-L. A., 2006, "Extending displacements of comb drive actuators by adding secondary comb electrodes," Journal of Micromechanics and Microengineering, pp. 684.
[21] Zhou, G., and Dowd, P., 2003, "Tilted folded-beam suspension for extending the stable travel range of comb-drive actuators," Journal of Micromechanics and Microengineering, 13(2), pp. 178-183.